International Journal of Nanoelectronics and Materials

In Press, Accepted Manuscript – Note to user

Effect of synthesis process on the piezoelectric properties of (1-x) NBT-xBT: a comparative study between solid state and hydrothermal method

M. Mesrar[1], A. Elbasset[1], F. Abdi[1], N-S. Echatoui[1] and T. Lamcharfi[1]

[1] Signals, Systems and Components Laboratory (LSSC), Faculty of Sciences and Technologies of Fez, Sidi Mohamed Ben Abdellah University, B.P. 2022, Fez, Morocco

Received 21 April 2022, Revised 5 September 2022, Accepted 12 September 2022

ABSTRACT

Lead-free oxide perovskite materials are produced to ensure that no toxic or dangerous waste is released into the environment, although this technique often requires a high-temperature synthesis method. Nevertheless, the development of an environmentally friendly chemical process to carry out the synthesis of perovskite material in the laboratory at low temperature is a major challenge. In this investigation, to lower the temperature of the thermal treatment, (1-x)($Na_{0.5}Bi_{0.5}$)TiO_3-x$BaTiO_3$ (abbreviated as (1-x)NBT-xBT) ceramics were synthesized using two different methods: a hydrothermal method and a conventional calcination process (solid-state), using the same reagents. The effects of various synthesis techniques on the composition, structure, morphology, and dielectric properties of the (1-x)NBT-xBT ceramics were registered and examined. The XRD plots taken at ambient temperature were used to verify the phase formation of the samples. The occurrence of functional bands was also verified by Raman spectroscopy at ambient temperature. Using the Rietveld refinement method were able to detect the morphotropic phase boundary (MPB) near x=0.05-0.07. When the hydrothermal process was adopted, the (1-x)NBT-xBT ceramics show a single perovskite structure sintered at 1000°C. Moreover, scanning Electron Microscopy (SEM) examination revealed a uniform distribution of grains and a significant change in grain size with the increase in $BaTiO_3$ concentration when compared to the conventional method. The microstructure of ceramics is generally strongly influenced by the method used to prepare the powders, which has a considerable impact on their performance. Piezoelectric and dielectric properties of the specimens have been compared with the properties of those prepared by the hydrothermal process. Thus, the choice of the suitable synthesis method depends on the desired properties of the (1-x)NBT-xBT materials.

Keywords: *(1-x)NBT-xBT*, Dielectric measurements, Hydrothermal method, Piezoelectric properties, Rietveld refinement, Raman Spectroscopy.

1. INTRODUCTION

In recent years, environmental concerns have intensified due to global warming and climate change. [1][2] Therefore, it is strongly advised to develop non-toxic components in order to avoid lead-based ferroelectric materials in various equipment, such as, for example, actuators, transducers, filters, multilayer capacitors, etc.[3][4]

Since bismuth is similar to lead in both mass and the outermost electron layer, it is likely to be used in place of lead in ferroelectric materials.[5] A considerable amount of research and development has been focused on the industrial applications of *(1-x)($Na_{0.5}Bi_{0.5}$)TiO_3-x$BaTiO_3$ (abbreviated as (1-x)NBT-xBT)* samples in various electromechanical devices and the high-density storage instruments such as *$Na_{0.5}Bi_{0.5}TiO_3$ (abbreviated as NBT)* provide the possibility that its electrical properties could be affected by the addition of several other combinations of ions on A site and/or on high valence B site of the ABO_3 perovskite structure.[6][7] In addition, the (1-x)NBT-xBT that is very near the morphotropic phase boundary (MPB) has been largely examined

based on its excellent dielectric and piezoelectric properties.[8][9][10]. The study of the structure of a material is a necessary condition to identify its qualities, and the choice of an appropriate synthesis process is crucial to determine the properties of the desired material. [1][11]

The solid-state method is an approach that mainly consists of calcining mixtures of stoichiometric products ($BaCO_3$, Na_2CO_3, Bi_2O_3, and TiO_2) at 1000°C. The alteration of the synthesis route, thermal treatment or processing condition in these ceramics also yielded quite radical results with regard to the structural and dielectric properties. [12][13][14] Moreover, these properties depend greatly on the ratios between the metallic elements, impurities, microstructure, and grain sizes.[15]

(1-x)NBT-xBT ceramics have been widely developed by solid-state reaction process utilizing oxides as the starting materials requiring a high calcination temperature to form the perovskite phase who normally leads to particle coarsening and aggregation, which is accountable for poor microstructure and consequently, the electrical properties of the (1-x)NBT-xBT ceramics will be degraded.[16] Furthermore, the high volatility of Bismuth and sodium (offset A-site cations) due to high-temperature (~1000°C) calcination generates another synthesis problem. Besides, in this case, a large excess of Bi_2CO_3 was incorporated to counteract the evaporation of the oxide.[17] Such a large excess of Bi_2CO_3 is susceptible to difficulties in adjusting the final product composition and may lead to degradation of the electrical properties of (1-x)NBT-xBT ceramics. [18]

To correct this problem, several wet chemical routes are also explored to produce (1-x)NBT-xBT powders at lower synthesis temperatures with high chemical homogeneity. This includes sol-gel process, the chemical co-precipitation method, solvothermal, and hydrothermal methods.

Between them, the hydrothermal process has the advantages of synthesizing micro-size powder with good crystallinity, high dielectric constant, and chemical activity in a process that is difficult to manage, but it allows better purity and homogeneity of the compounds to be obtained compared to high-temperature calcination (solid-state method).[19]

This is because hydrothermal crystallization occurs as a self-purifying mechanism, at the moment when the growing crystals/crystallites will tend towards rejecting the impurities contained in the growth environment, which does not occur during other synthesis routes, such as solid-state. [20][21]

A considerable advantage of hydrothermal synthesis is that the low reaction temperatures (T≤200ºC) also avoid the difficulties mentioned earlier regarding high-temperature treatments, for instance, inadequate control of stoichiometry due to volatilization of components (e.g., Bi volatilization in ceramics). [17][22]

Therefore, in order to clarify the morphology mechanism of (1-x)NBT-xBT particles in hydrothermal synthesis, a more detailed examination is needed. It should be remembered that a few reports of comparative studies are published in the literature [11][23], exploring the relationship between the sintering conditions and the piezoelectric properties of these materials alone.

In this work, (1-x)NBT-xBT ceramics were prepared by the hydrothermal process and solid-state method, respectively. The influence of synthesis parameters on the phase structure of (1-x)NBT-xBT compounds has been examined in a systematic approach. The structural, microstructure, dielectric, ferroelectric, and piezoelectric properties obtained from hydrothermal, and solid-state synthesized (1-x)NBT-xBT materials were discussed and compared. In addition, experiments with relative piezo-response were explored as a means of gathering information on domain patterns and mechanical properties. This work enables the implementation of a simple and environmentally friendly preparation method for high-quality (1-x)NBT-xBT ceramics.

2. Experimental

2.1. Sample preparation

In the present research, all reagents (oxides and carbonates) were obtained in an analytical grade from commercial sources without any further purification.[24][25] The perovskite-type (1-x)NBT-xBT (x= 0.00; 0.03; 0.05; 0.06; 0.07; 0.08 and 0.10) compounds were synthesized by employing a conventional solid-state reaction and hydrothermal route, respectively, and their structural and electrical properties were compared.

Solid-state reaction

Polycrystalline NBT specimens have been successfully produced by means of the solid-state route using the high-purity starting elements Bi_2O_3 and TiO_2 (AppliChem GmbH; 99.97%) and the carbonates $BaCO_3$, Na_2CO_3 (AppliChem GmbH; 99.97%). The powders in the stoichiometric ratios were carefully ground in an agate mortar in acetone medium and then calcined at different temperatures (800, 900 and 1000°C) for 4 hours in order to determine the optimal temperature for the formation of pure phase, with a temperature increase at a rate of 3°C/min, then a cooling which follows the inertia of the furnace until room temperature. The specimens have been pressed using 2% polyvinyl alcohol as a binder at a pressure of 6 tons for 3min into disks of a suitable size and subsequently sintered at 1100°C in air in a regulated furnace for 4 hours. The details of the treatment conditions are provided elsewhere.[17]

Hydrothermal process

Bismuth oxide (Bi_2O_3), barium carbonate ($BaCO_3$), and titanium oxide (TiO_2) have been employed as bismuth precursor, barium precursor and titanium elements respectively. Sodium hydroxide (NaOH) was employed as a sodium precursor and mineralizer. For the hydrothermal synthesis of NBT, stoichiometric amounts of the starting products were carried out in a Teflon autoclave (50 mL) in the presence of NaOH solution (10 M). The reaction temperature was at 200 °C and the reaction duration was 24 h. The autoclave has been allowed to cool to ambient temperature naturally after the reactions have been finished. The materials underwent filtration, and were washed several times with distilled water and allowed to dry at 80 °C overnight (see Figure 1). Hydrothermally synthesized NBT ceramics were then mixed with 2.0 wt% polyvinyl alcohol (PVA) as a binder and plasticizer, then pressed into discs with a diameter of 12.0 mm and a thickness of 1.5 mm. The pellets were sintered at 1000 °C for 4 hours at ambient room temperature. The mean diameter and thickness of the sintered specimens consisted of 10.0 mm and 1.0 mm, respectively .[26]

2.2. Characterization of NBT

XRD analysis: The crystal structure of the different materials has been established by means of X-ray diffraction (XRD) measurements with a (XPERT-PRO; CuKα radiation: λ=1.54 06Å). Crystallite sizes, crystal fractions, lattice constants and weight fractions have also been derived from Rietveld fitting of the diffraction results.

Raman spectroscopy measurement: The relationship between the Raman band and various types of atomic interaction was investigated using a Raman spectrometer equipped with a monochromatic light source of wavelength 410 nm. After sample processing, the Raman spectra were registered at room temperature.

Scanning electron microscope measurement: Pellets are sintered at 1100°C for 4 hours after being uniaxially pressed in a cylindrical mold (d= 12mm) at a pressure of around 10 tons, and then polished with extremely fine abrasive paper to make the two surfaces flat and parallel. Scanning electron microscopy (SEM) (Quanta 200) was used to examine the grains' microstructural and morphological properties at a 10 kV accelerating voltage.

Dielectric properties measurement: An Agilent impedance analyzer was used to investigate the temperature-dependent dielectric characteristics of solid solutions at frequencies up to 1MHZ and temperatures up to 600°C.The zview impedance software has been employed to fit the experimental impedance measurements.

Piezoelectric properties: Using a resonant-antiresonant frequency approach, the electromechanical coupling factor (kp) was calculated.

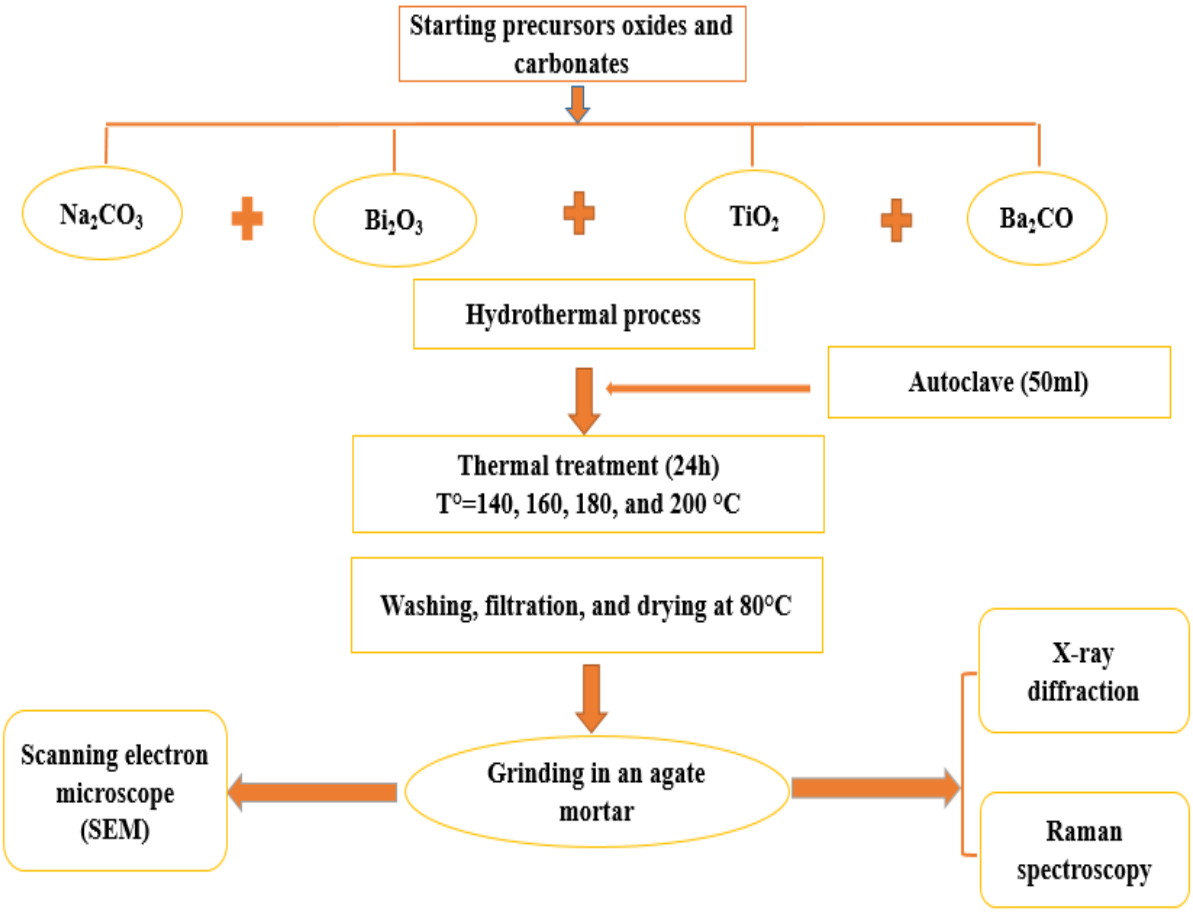

Figure 1. Graphical depiction of all the steps in the synthesis of (1-x)NBT-xBT samples

3. Results and discussion

3.1. Phase Identification Analysis

3.1.1. Preparation of $(Na_{0.5}Bi_{0.5})TiO_3$ through solid-state technique

X-ray diffraction (XRD) analyses were also performed to determine the formation of crystalline phases, the degree of crystallinity and the crystallite size of the different powders obtained by both methods. The NBT specimens, which have been produced according to the solid-state process, is calcined at different temperatures ranging from 800 to 1000°C for 4 hours to obtain the best possible calcination temperature. Figure 2 illustrates the appropriate XRD patterns. From Figure 2, it is noticed that the NBT phase formation occurs at a temperature of 800°C. With increasing temperature, the percentage of the secondary phase decreases and the NBT phase increases. Moreover, the peaks correlated to the secondary phases are $Bi_4Ti_3O_{12}$ (JCPDS No.35-0088) [27][28] and $Bi_2Ti_2O_7$ (JCPDS No.32-0118)[29] were also identified with low intensities (marked with an asterisk), which is caused by insufficient reaction temperature between the initial reagents Bi_2O_3 and Na_2CO_3.

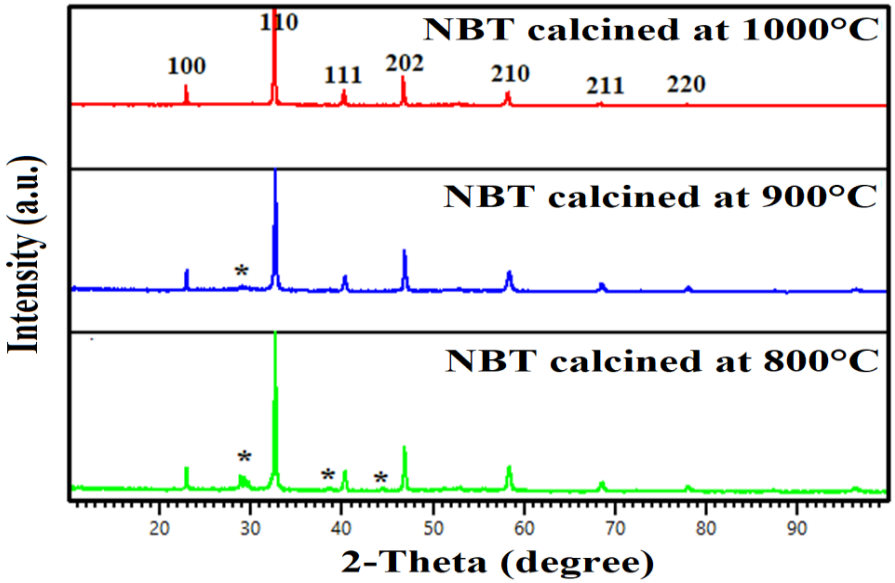

Figure 2. X-ray diffraction (XRD) pattern of NBT specimens treated at various temperatures (800, 900, and 1000°C) employing solid-state techniques

The intense peaks in this product's XRD diagram, which was calcined at 1000°C for 4 hours, are indexed to distinct NBT (h k l) planes, and a rhombohedral NBT structure with an R3c space group has been identified. This indexing corresponds to the JCPDF data file (No.01-070-9850). Moreover, the calcination temperature of the solid-state processed samples is finally optimized to 1000°C for 4 hours to achieve better phase formation for this investigation.

3.1.2. Preparation of $(Na_{0.5}Bi_{0.5})TiO_3$ through hydrothermal process

The nucleation and crystal growth process of NBT perovskite is controlled by the reaction rate that is tied to the reaction temperature in the hydrothermal synthesis process. The hydrothermal temperature is established at 140, 160, 180, and 200 °C for 24 hours to investigate the effect of hydrothermal temperature on the structure evolution of the NBT samples, with 10M of NaOH. As revealed in Figure 3, with a reaction temperature between 140°C and 180°C, even if there is a predominance of perovskite phase in the different samples, we note the presence of a faint diffraction peak of the secondary phase $Bi_4Ti_3O_{12}$[27][28] (marked with a round black circle). Moreover, when the hydrothermal temperature rises to 200°C, all the diffraction peaks correspond well to the ones of the perovskite phase of NBT, and no second phase could be identified. The results obtained suggest that increasing the reaction temperature leads to a greater vibrational velocity of Na^+, Bi^{3+} and Ti^{4+} ions, this has the consequence of increasing the number of effective collisions between these ions and the increase of the reaction activation energy. Since the Teflon lining of our autoclave can only withstand temperatures of 200°C, it is more appropriate to set the reaction temperature at 200°C.

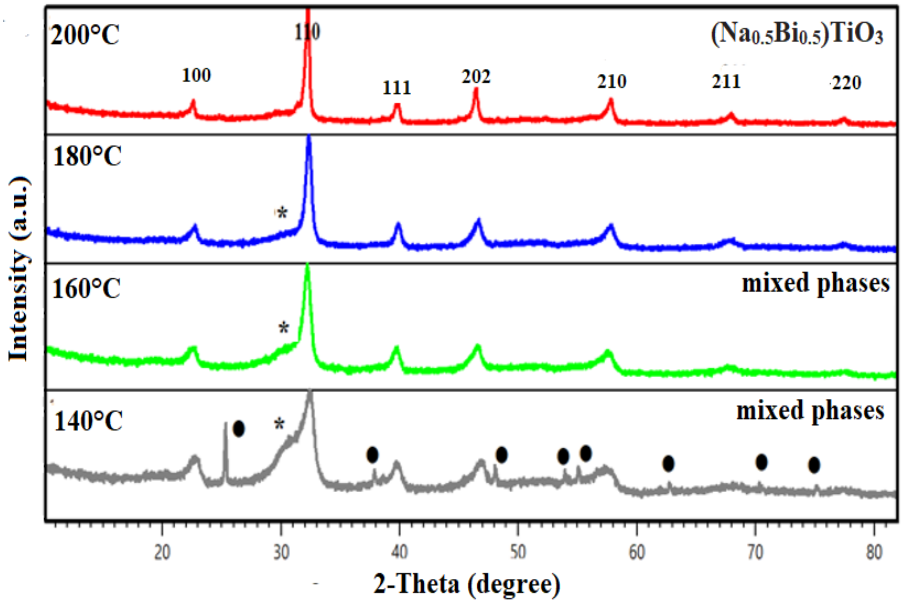

Figure 3. X-ray diffraction (XRD) pattern of NBT specimens prepared by hydrothermal process, treated at different temperatures (140, 160, 180 and 200°C)

However, the synthesis temperature of the pure NBT sample produced via the current hydrothermal technique is significantly lower than that needed for the solid-state method. Moreover, it is observed that there is no intermediate phase of $Bi_2Ti_2O_7$ [27] pyrochlore produced in the present hydrothermal technique, this could be due to a different pathway in the formation of the perovskite phase than the solid-state method, and the exact reason is still being investigated. Hence, in contrast to the conventional solid-state calcination approach, the hydrothermal process leads to the formation of a nearly single-phase NBT at approximately (~200°C) much lower temperature.

3.1.3. Rietveld Refinement analysis

Following that, using the "FULLPROF" software, the diffraction data are subsequently treated by the Rietveld refinement method. The Refinement on the composites elaborated in the solid-state and by the hydrothermal process is realized assuming a rhombohedral structure with a space group R3c and a good fit was obtained. Depending on the outcomes of the refinement of the rhombohedral phase, a polyhedral model for each sample has been created through the use of Diamond software [30] and displayed beside the plots of Figures 4a and 4b. The refined lattice parameters are included in a full list of crystal structure parameters in Tables 1 and 2. The natures and typical behavior of these parameters are: Based on the following table, you can see that there is a difference in the lattice parameters that are obtained as between solid-state and hydrothermal processes. Moreover, the unit cell lattice parameters for the NBT (solid-state) synthesis is larger as compared to NBT (hydrothermal). Additionally, the tetragonality defined as (c/a), present a small difference. This could be explained by a correlation between the unit cell and the high calcination temperature (solid-state), which is mainly responsible for a decrease in deformations and defects and thus more room for NBT crystal to get organized and hence the volume gets higher. Hence, this suggests that the calcination temperature has a substantial impact on the phase structure of the NBT samples.

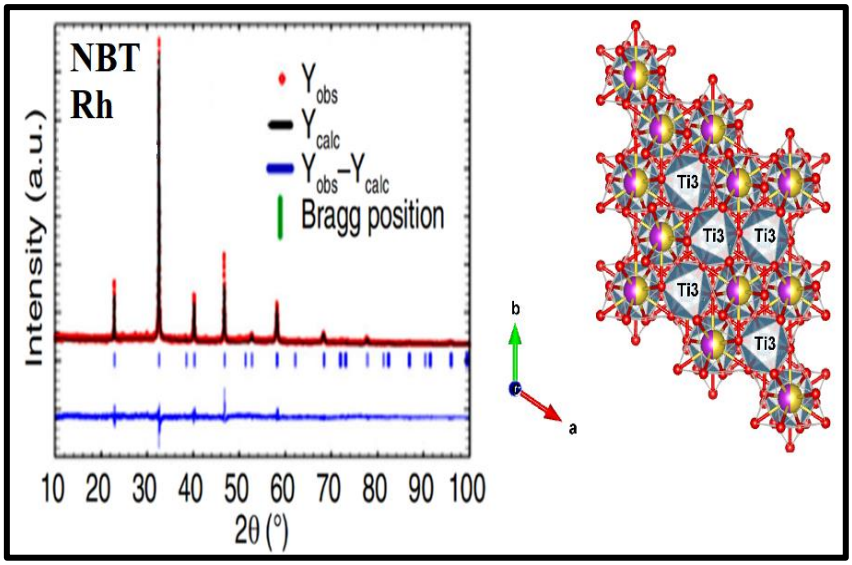

Figure 4a. Rietveld refinement for $(Na_{0.5}Bi_{0.5})TiO_3$ specimens calcined at 1000°C

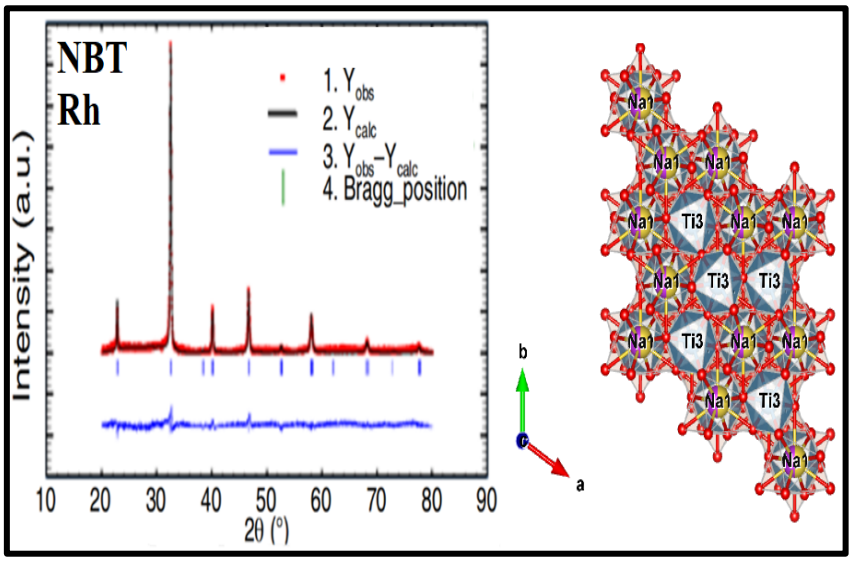

Figure 4b. Rietveld refinement for $(Na_{0.5}Bi_{0.5})TiO_3$ specimens treated at 200°C

Using the Scherrer' equation ($d = 0.9\lambda/\beta\cos\theta$) and the entire width at half maximum (FWHM), we calculated the crystallite sizes of NBT. The XRD plots in Figures 2 and 3 for the NBT (hydrothermal) sample exhibit a broad peak, meanwhile the XRD plot for the NBT (solid-state) specimen shows very sharp and narrow peaks. The crystallite sizes (161.31nm) of NBT–hydrothermal were clearly smaller than those (165.23 nm) of NBT–solid-state. The Rwp=3.67% and Rwp=3.65% for solid-state and hydrothermal refinements, respectively, at room temperature, confirm a very good refinement.

Table 1 Structural refined characteristics of NBT produced in solid-state and hydrothermal processes

NBT	Solid-state	Hydrothermal
a (Å)	5.4915	5.487
b (Å)	5.4915	5.487
c (Å)	13.5206	13.5050
c/a	2.4621	2.4613
V (Å³)	353.11	352.12
Z	6	6
Crystalline grain size (nm)	165.23	161.31
Space group	R3c Rhombohedral	R3c Rhombohedral
Rwp (%)	3.67	3.25

Table 2 Refined structural parameters for solid-state and hydrothermal process NBT

Atoms	Wyck off	Coord-inates	Solid-state	Hydrothermal
Na/Bi	6a	x	0	0
		y	0.500	0.545
		z	0.273	0.268
Ti	6a	x	0	0
		y	0	0
		z	0.0091	0.0087
O	18b	x	0.12651	0.13521
		y	0.33923	0.34344
		z	0.08333	0.08333

3.1.4. XRD analysis for (1-x)NBT-xBT

Figures 5(a-b) and 6(a-b) exhibit the X-ray diffraction (XRD) patterns of (1-x)NBT-xBT, as well as their Rietveld refinement. The Rietveld refined XRD diagrams have been established utilizing the pseudo-Voigt function to characterize the peak profiles. The goodness of fit (Rwp) values were used to validate the fitting quality. All materials for both methods exhibit a pure perovskite structure phase and no secondary phase could be identified, is implying that Ba^{2+} has diffused through the NBT lattice and formed a solid solution. [31][32][33][34] The XRD peak splitting in the 2Θ region of 45.5º-47.5º for various compositions is shown in Fig. 5(b).

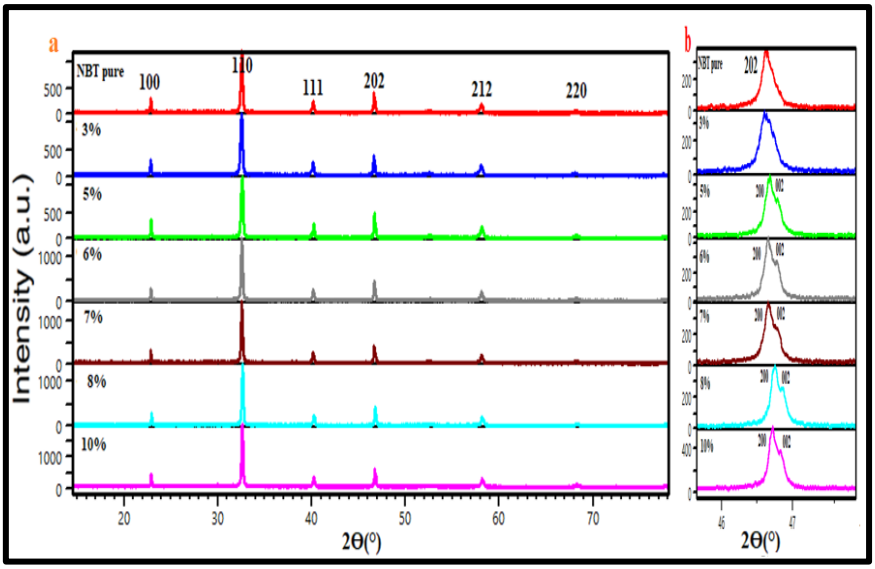

Figure 5. (a) X-ray diffraction plot of the product (1-x)NBT-xBT –(solid-state); (b) Zoom of the peak (202) in the 45-47° range [17]

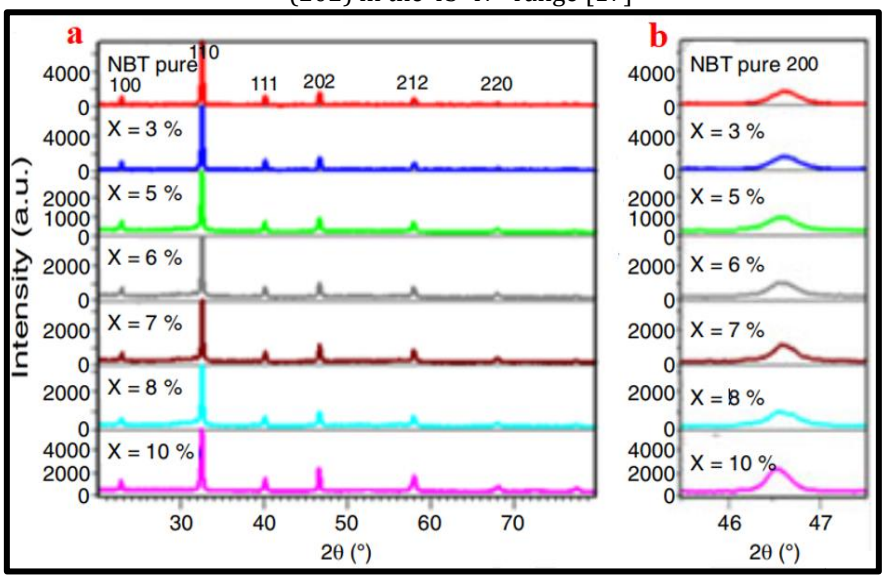

Figure 6(a). X-ray diffraction diagram of the ceramic (1-x)NBT-xBT compounds hydrothermally (b) Zoom of the peak (202) in the 45-47° range [35]

Both peaks, designated $(200)_R$ and $(002)_T$, correspond to the rhombohedral and tetragonal phases, respectively. and the appearance of the morphotropic transformation phase (MPB) around x = 0.05 was confirmed, which is consistent with current literature.[36][37] By means of the refinement study (see figure 7 and 8), it was observed that all synthesis methods had a morphotropic phase boundary (MPB) in the composition region of x= 0.05-0.07 (see table 3). Consequently, when comparing to the solid-state method, the hydrothermal process results in the formation of the morphotropic phase boundary (MPB) near x= 0.05-0.07 at a much lower temperature (200°C). The variation in lattice parameter values of hydrothermal synthesis when compared to conventional calcination (solid-state) around MPB composition (see table 3), may be related to the effect of reaction kinematics and internal stress on lattice crystallization, compared to solid-state samples.

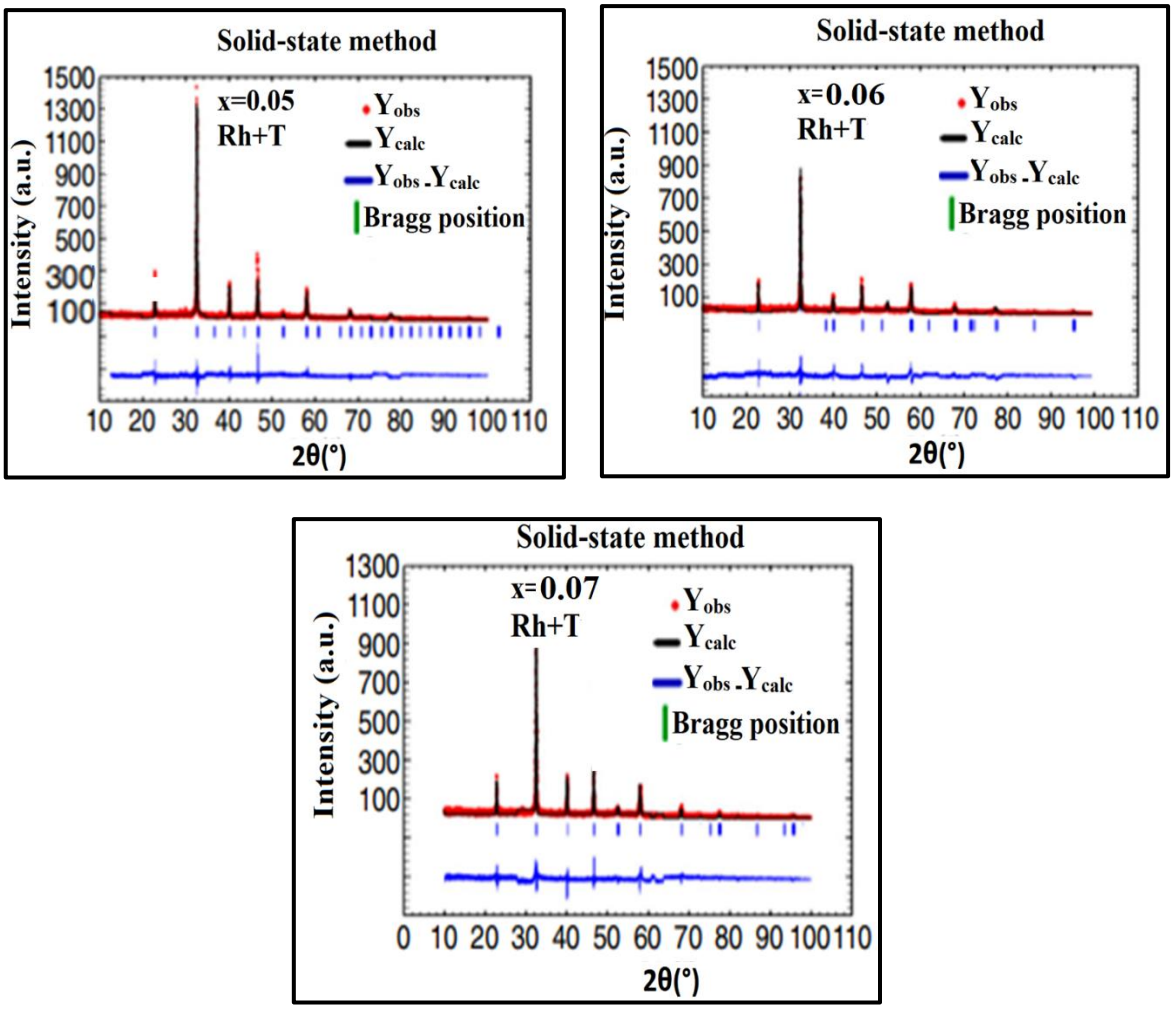

Figure 7. Rietveld refinement for materials (1-x)NBT-xBT –(solid-state) calcined at 1000 °C. [17]

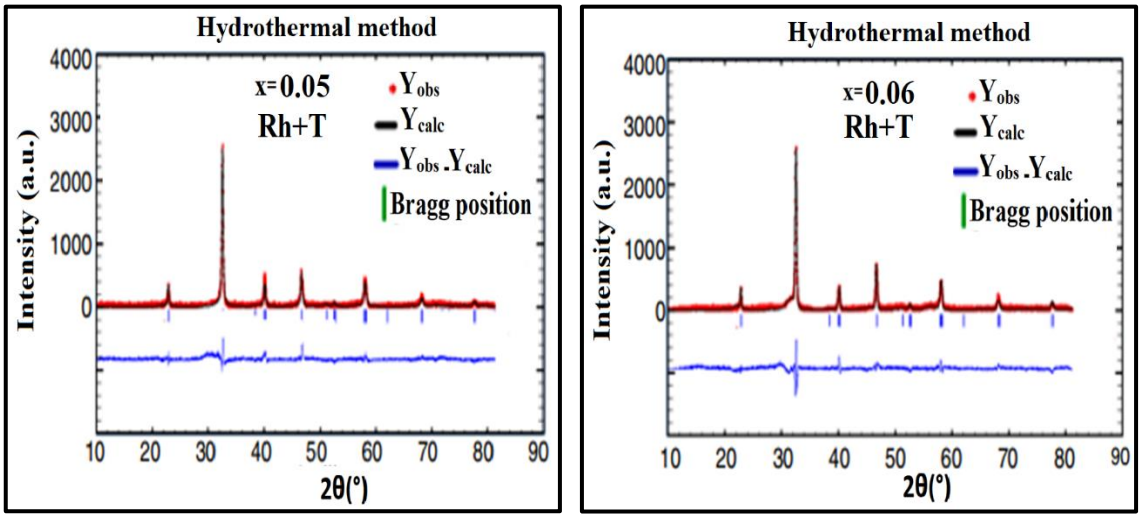

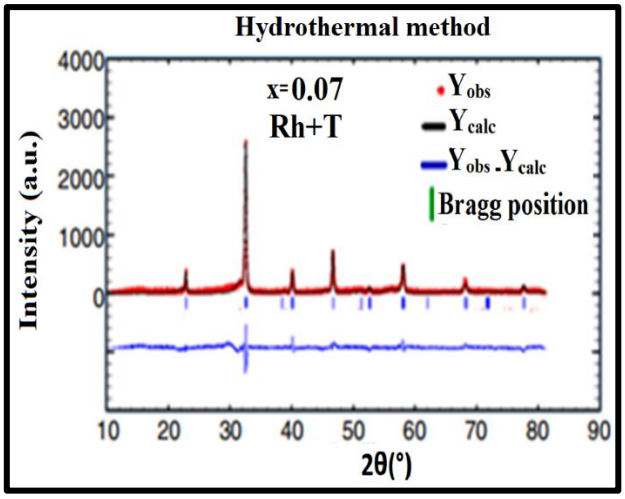

Figure 8. Rietveld refinement for materials (1-x)NBT-xBT–(hydrothermal) treated at 200 °C. [35]

Table 3 The lattice parameters of (1-x)NBT-xBT materials by refinement

xBT	Phase fraction (%)	Lattice parameters Hydrothermal			Lattice parameters Solid-state		
		a (Å)	**b** (Å)	**c** (Å)	**a** (Å)	**b** (Å)	**c** (Å)
0.05	R3c 70.125% P4bm 29.875 %	5.501 5.498	5.501 5.498	13.488 3.910	5.508 5.497	5.508 5.497	13.516 3.9001
0.06	R3c 68.267% P4bm 31.733 %	5.514 5.514	5.514 5.514	13.492 3.930	5.528 5.5179	5.528 5.5179	13.517 3.910
0.07	R3c 69.763 % P4bm 30.237 %	5.519 5.515	5.519 5.515	13.514 3.941	5.528 5.5154	5.528 5.515	13.549 3.923

3.3. Raman Spectroscopy studies

The influence of different synthesis routes will be examined using Raman scattering that will provide valuable information about the lattice vibrations and crystal structure. The Raman modes of NBT obtained via solid-state and hydrothermal methods are illustrated in figure 9 ((a) and (b)). The irreducible representation of optical phonon for the NBT structure possessing the rhombohedral structure with R3c symmetry is Γvib= 4A1+5A2+9E where A1, E modes are the Raman and infrared active modes, while the A2 mode is both Raman and infrared inactive generating a total of 13 Raman active optical phonon modes 25. For NBT-solid-state, four bands, located at about 137.47, 283.86, 532, 580 and 866 cm^{-1} are visible.

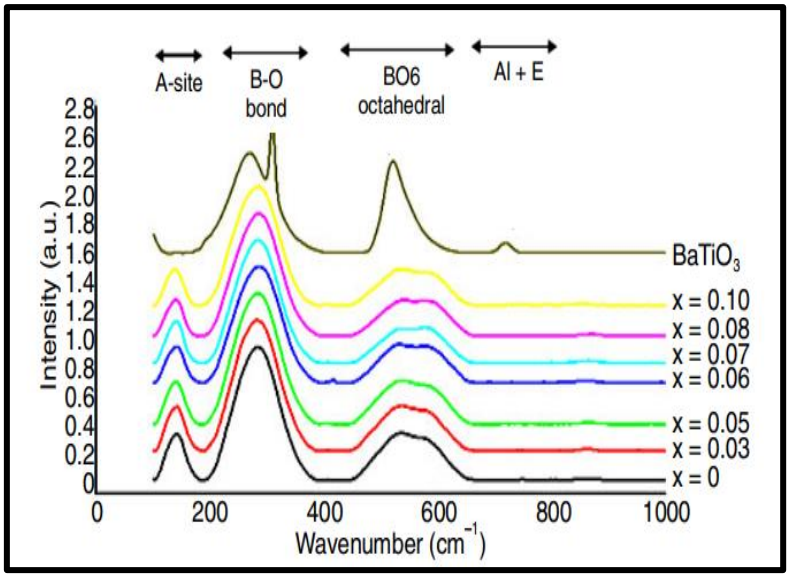

Figure 9(a). Raman spectra of various compositions of (1-x)NBT-xBT ceramics (solid-state) [17]

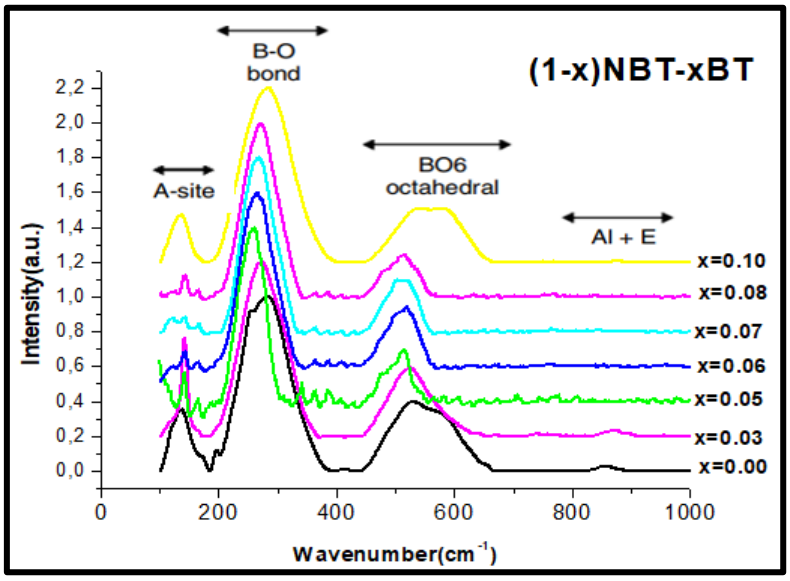

Figure 9(b). Raman spectra of various compositions of (1-x)NBT-xBT ceramics (hydrothermal). [35]

The frequencies of occurrence of these modes are consistent with the ones of the rhombohedral R3c NBT reported in the literature. The identified peaks are divided into three groups of wave numbers. There are (1) low wavenumber range of 100–200 cm^{-1} that is considered to be associated with Na–O and is attributed to the A1 (TO1) mode symmetry. (2) A mid wavenumber region of 200–400 cm^{-1} that is considered associated with Ti–O which are then attributed to E(TO2) symmetry. This band is highly impacted by all structural transitions. (3) A wavenumber range of 400–600 cm^{-1} that appears to be associated to TiO_6 octahedra, the splitting of these peaks in this range suggests that there are two types of A–BO_6 interactions in the NBT material. (4) A high wavenumber at around 800cm^{-1}, which would be associated with oxygen octahedral vibrations and rotations. In addition to this, similar kind of Raman features was found in the hydrothermal method, in which a small shift at the center of these bands is revealed (135, 285, 530 and 866 cm^{-1}), respectively.

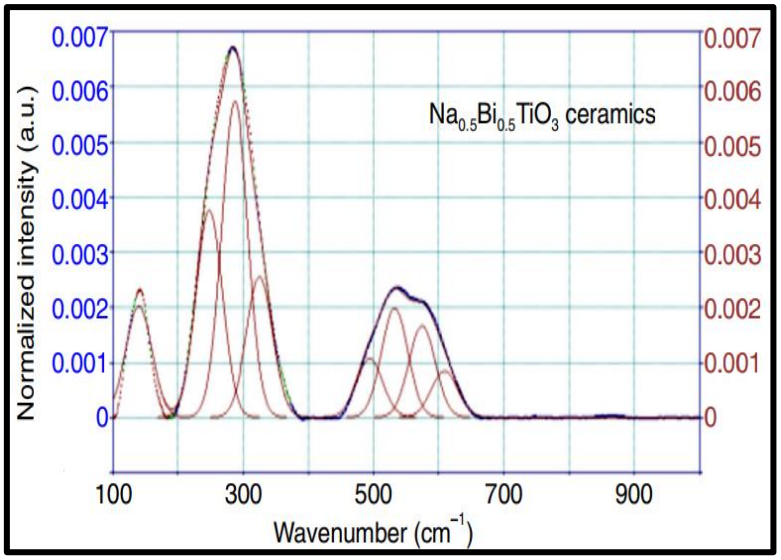

Figure 10(a). The deconvoluted Raman spectra of NBT ceramics (solid-state)

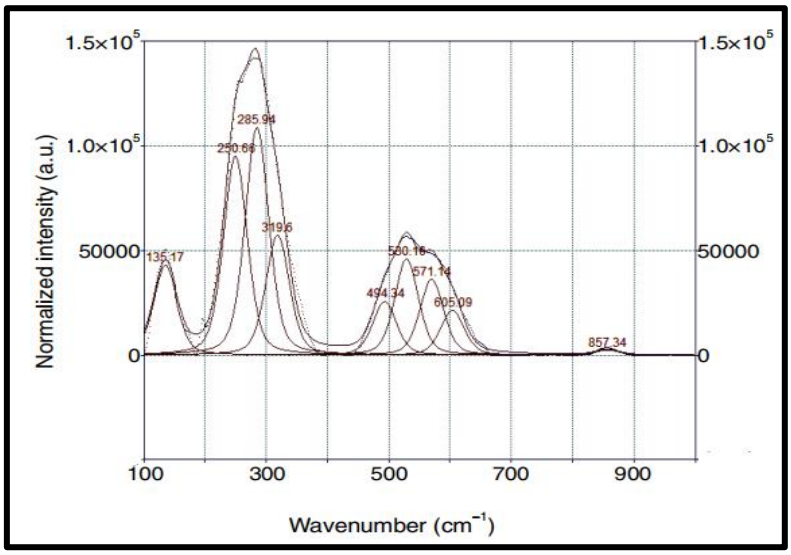

Figure 10(b). The deconvoluted Raman spectra of NBT ceramics (hydrothermal)

Therefore, the analyzed Raman modes are similar for both solid state and hydrothermally formed samples, apart from the variation in relative intensities. We used Peakfit software to deconvolve the pure NBT Raman spectrum in order to better understand the spectral development, with the Gaussian and Lorentzian area function as illustrated in Fig. 10(a and b). All modes revealed in this research are comparable to those previously discussed by Petzelt et al [38] and Wang et al[39].

3.4. Morphological studies

The scanning electron microscopy (SEM) image of the (1-x)NBT-xBT materials seen on the surface of the specimens is shown in Fig.11(a-b) and 12(a-b) in solid-state and hydrothermal, respectively. The microstructure of the samples reveals that they have an optimal density and minimal vacancies. The solid state material's microstructure is agglomerated, with grain sizes ranging from 4~5 μm for pure NBT. The hydrothermal ceramic has a grain size of ~20 μm on average, whereas solid state specimens have a grain size of (~4μm). In addition, the degree of densification of materials produced by different processes changes significantly. The densities of

the pellets obtained by the hydrothermal method and the solid state method are 5.980 g/cm^3 and 5.860 g/cm^3 respectively. Nevertheless, reduced pore size and higher grain size are two reasons that favor the increase in structural density. According to the different techniques, there is a clear variation in the average grain size of the samples. On the basis of these results, the grain size of samples elaborated by hydrothermal route is much higher with reduced porosity in these ceramics, than that of the ceramics sintered (1100°C) using a traditional furnace, which agrees with earlier findings.[40][41][42]

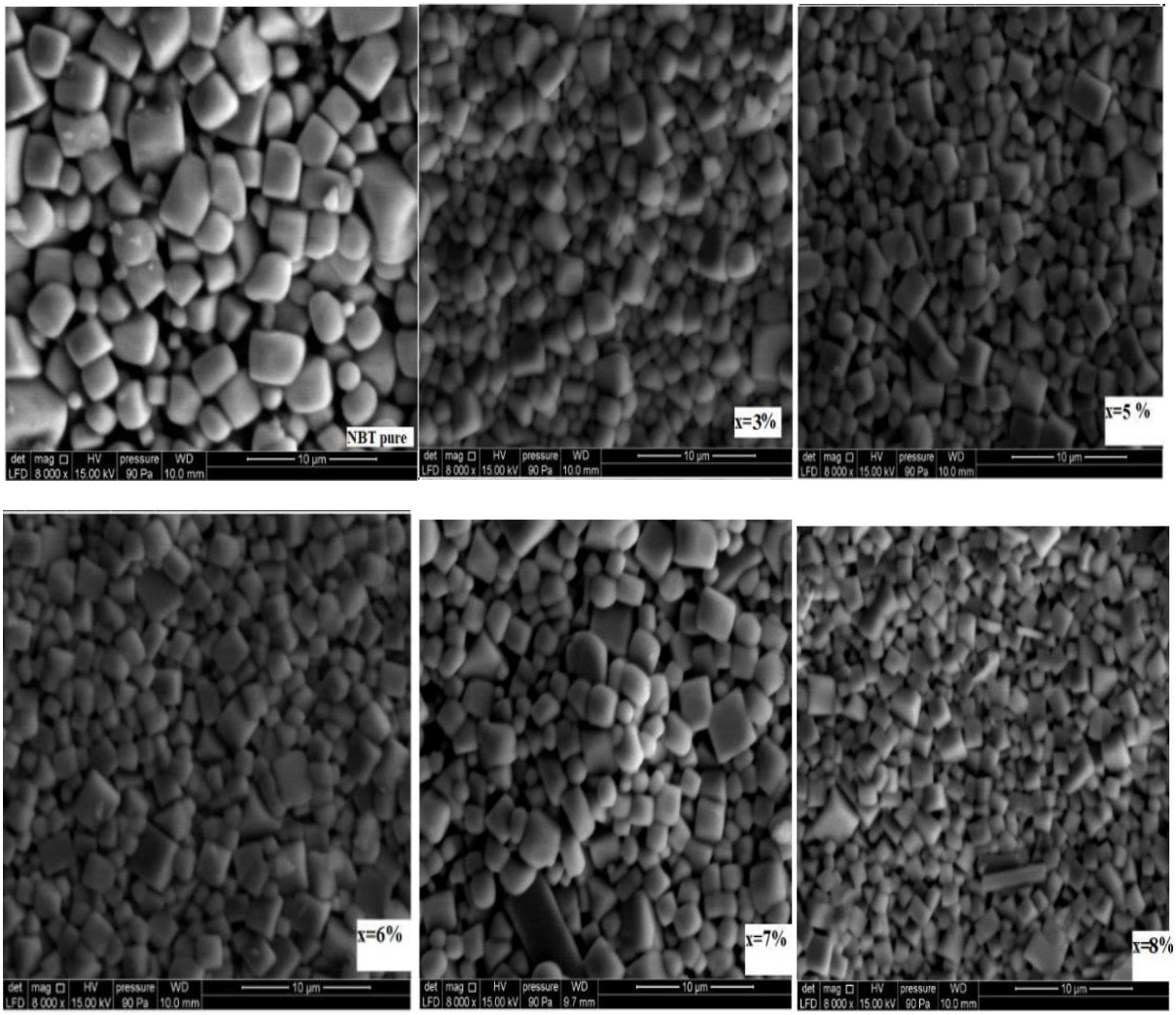

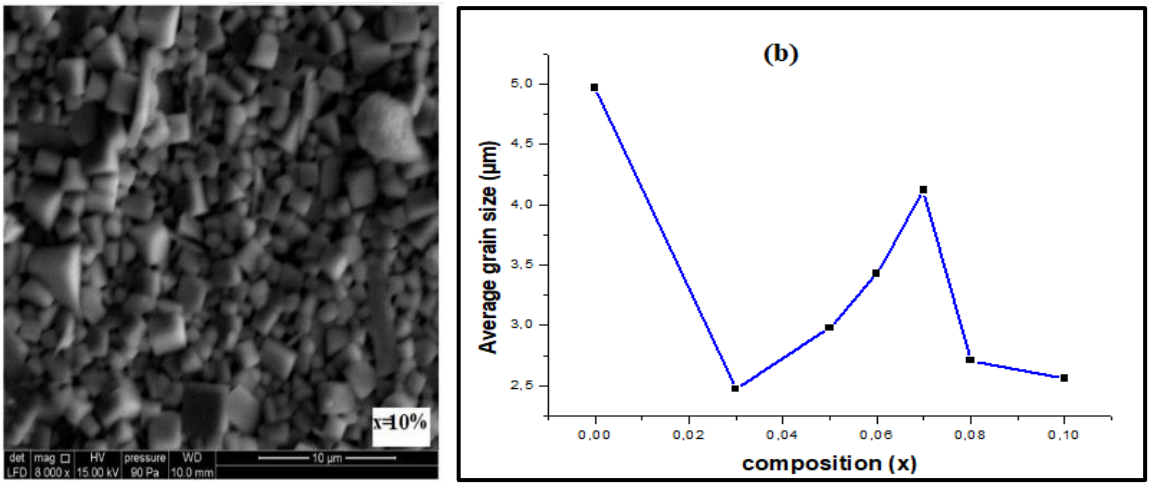

Figure 11(a). Cross-section SEM images of (1-x)NBT-xBT ceramics (solid-state, 10μm magnification) (b) Average grain size variation with compositions.[16]

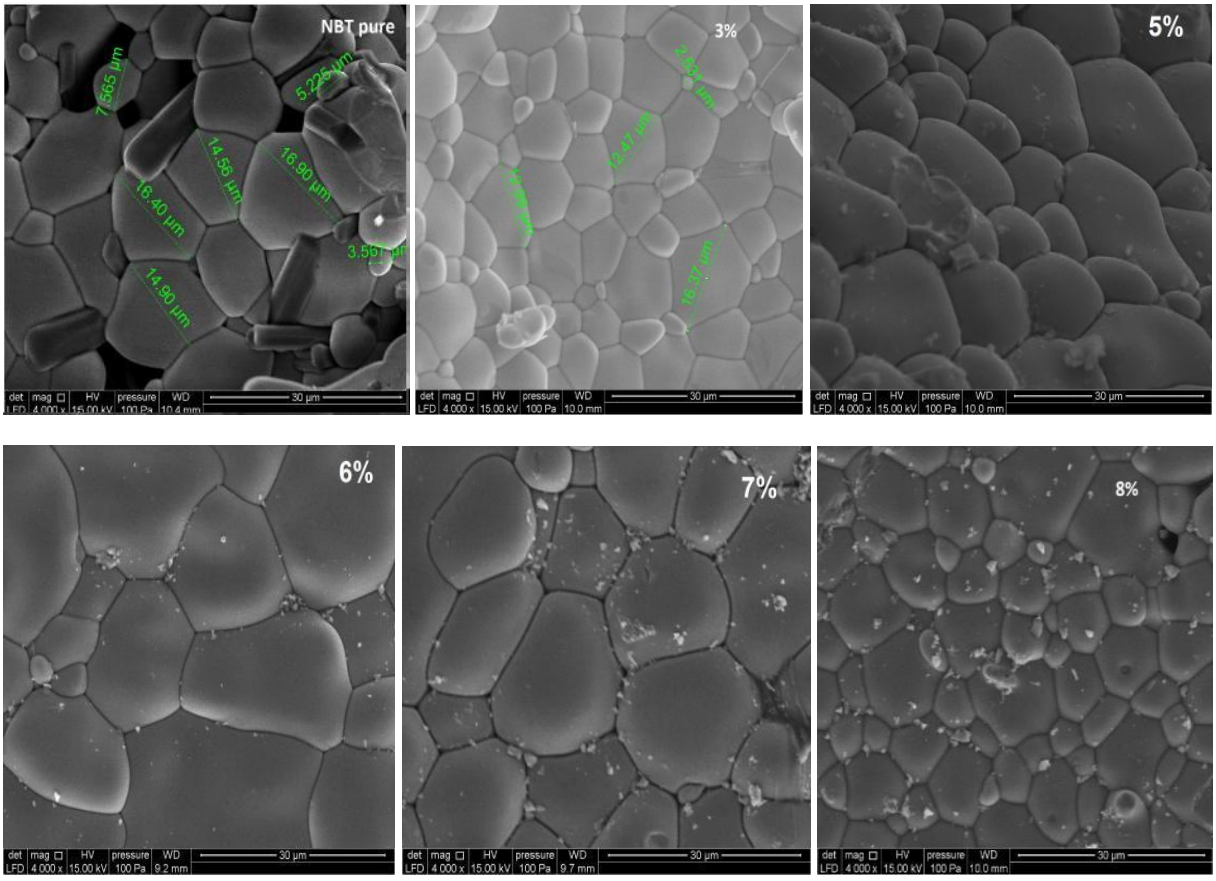

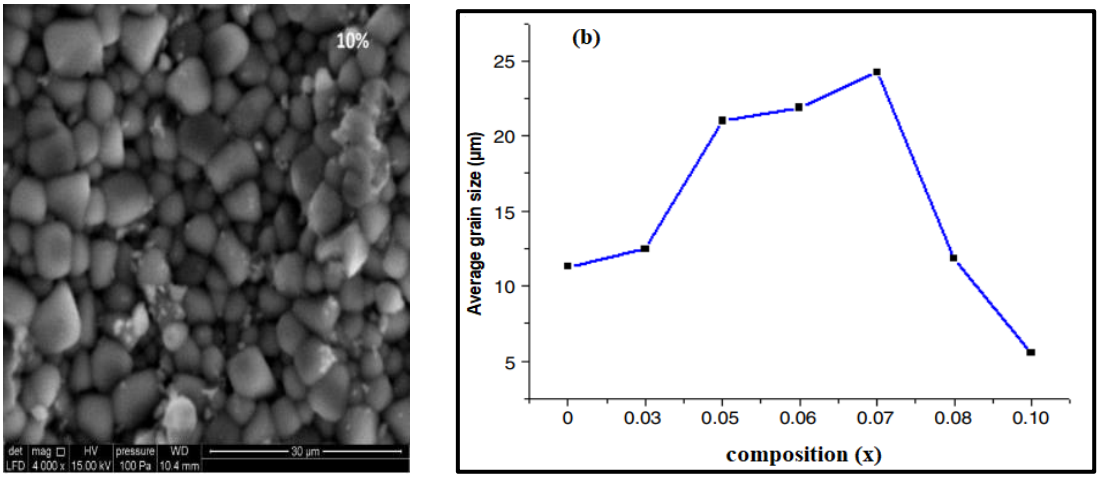

Figure 12(a). Cross-section SEM images of (1-x)NBT-xBT ceramics (hydrothermal, 10µm magnification) (b) Average grain size variation with compositions. [35]

3.5. Frequency dependent dielectric studies

Table.4 compares the dielectric characteristics of NBT ceramics made by our solid-state techniques to those of ceramics prepared by the hydrothermal approach. The frequency response of the relative dielectric constant (εr) and dielectric loss (tanδ) in a significant frequency region (500Hz-500kHz) for the compound NBT is shown in Fig.13(a-b) and 14(a-b) respectively at selected temperatures. The dielectric curves of the ceramics synthesized using solid-state reaction and hydrothermal process were found to be similar. It is clearly remarked from the (εr)-frequency curve (tanδ)-frequency plot that the relative permittivity and dielectric loss decrease with increase in frequency and essentially have a constant value at the higher frequencies for all methods of the synthesis.

Table.4 Dielectric properties of specimens produced via the hydrothermal and solid-state methods for NBT

Dielectric properties	Hydrothermal method	Solid-state method
ε_r	9549	1531
tanδ	0.085	0.087

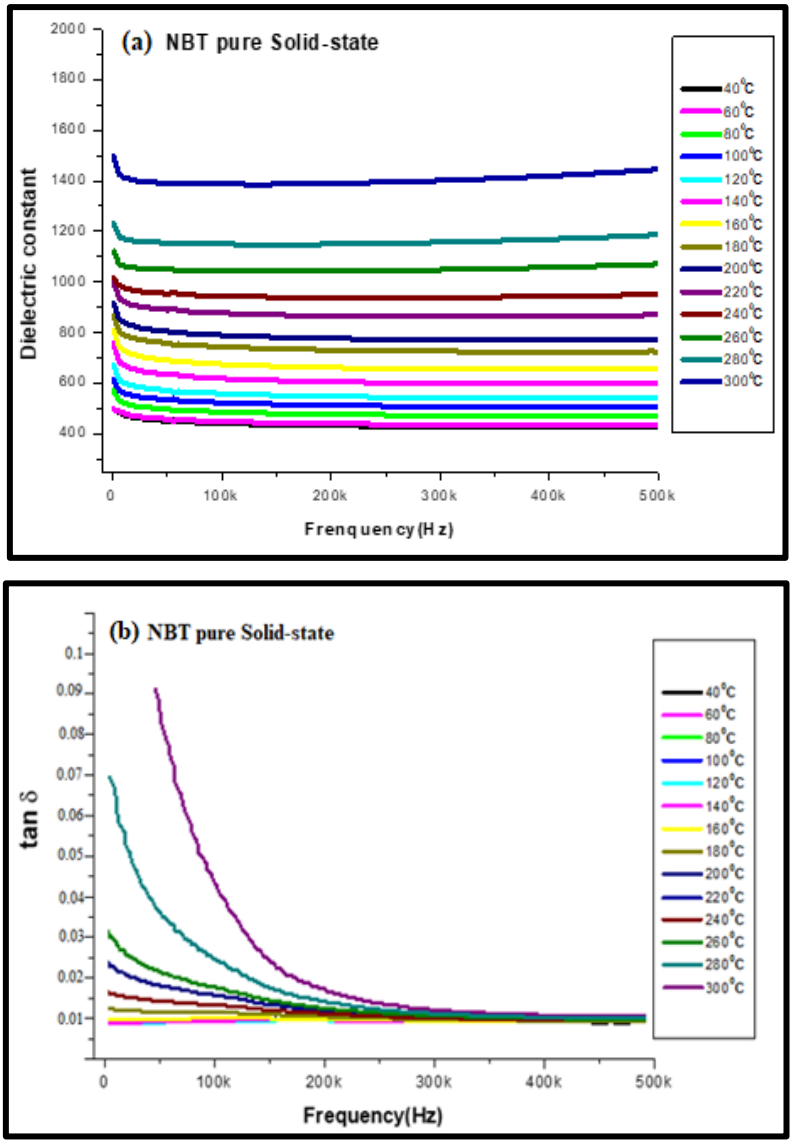

Figure 13(a). Frequency-dependence of dielectric permittivity (ε_r) of NBT sample; (b) tanδ of the samples increases with the temperature but reduces with frequency (solid-state).

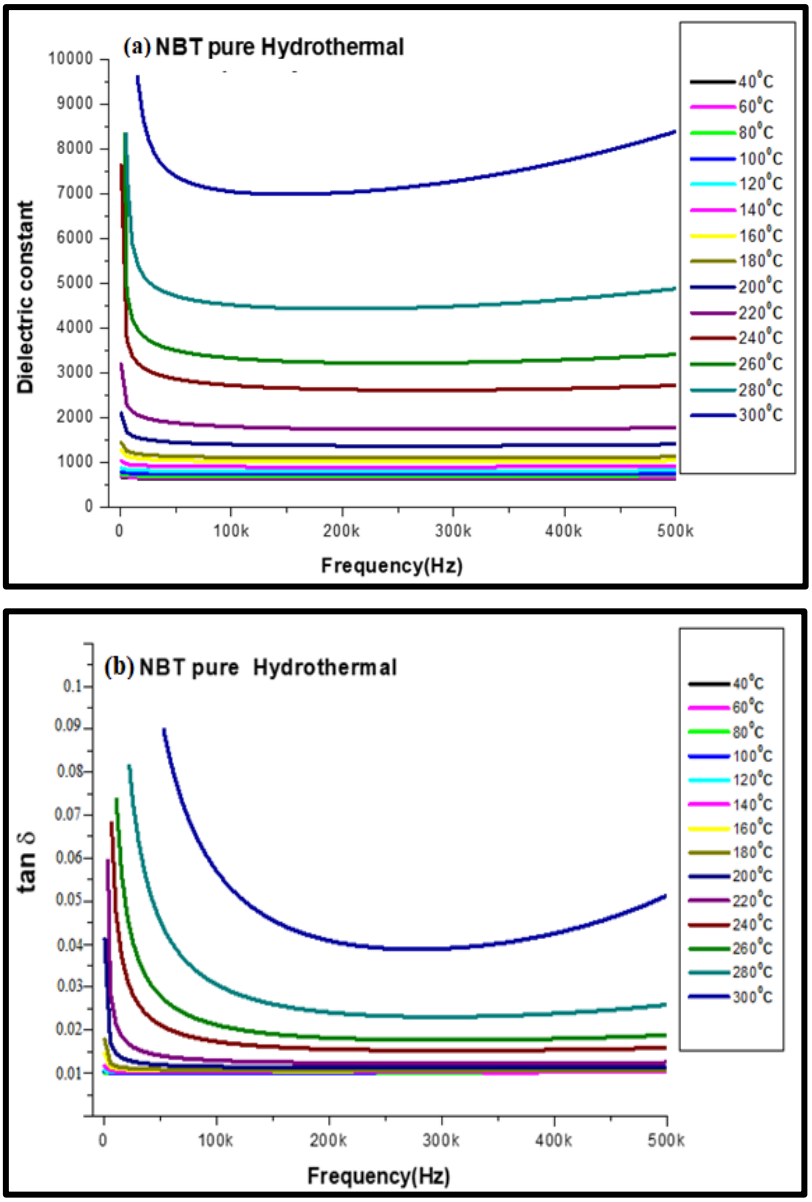

Figure 14(a). Frequency-dependence of dielectric relative permittivity (ε_r) of NBT sample; (b) tanδ of the samples increases with the temperature but reduces with frequency (hydrothermal)

The decrease of dielectric relative permittivity (ε_r) with increasing frequency appears to be attributable to the different polarization of ionic, electronic, dipolar, orientation and space charge polarization. In the low frequencies, the polarization of the space charge is dominant. Only the electronic polarization with a long relaxation period survives in the high frequency region, and all other polarizations vanish. When the pellets are sintered (1000°C) in the hydrothermal treatment, with a dielectric constant (ε_r) of 9549 and a dielectric loss (tanδ) of 0.085 (at 300°C), the ceramics exhibit the best dielectric characteristics. In addition, the increase in the dielectric constant with an increase in temperature generally comes from the increase in charge carriers blocked at the grain boundaries.[43][44] Hence, the maximum (ε_r) and minimum (tanδ) are obtained for the NBT ceramic synthesized by the hydrothermal process since the coarse-grained sample specimen results in a thinner layer of grain-boundary. The dielectric permittivity (ε_r) and dielectric loss

(tanδ) for all temperature exhibit normal behavior. According to an earlier study of Huang et al.[45]

3.6 Piezoelectric studies

For various approaches, Table 5 groups the values of the piezoelectric constant (d_{33}) and electromechanical coupling factor (k_p) of the NBT ceramics.[46] Electromechanical coupling coefficient, kp, is determined based on the resonance (fr) and anti-resonance (fa) frequencies, as shown in the equation (1),(2),(3) and (4):

$$K_p=[2.51*\frac{f_a-f_r}{f_r}]^{1/2} \quad (1)$$

$$K_{31=}[\frac{1-\sigma_E^2}{2}]\ K_p^2 \quad (2)$$

$$\frac{1}{S_{11}^E}=\frac{\pi^2 d^2 f_r^2(1-\sigma^E)\rho}{\eta_1^2} \quad (3)$$

Where $\boldsymbol{\sigma_E}$ corresponds to the Poisson factor ($\boldsymbol{\sigma_E}$ = 0.310), $\boldsymbol{\rho_1}$ corresponds to the Bessel equation ($\boldsymbol{\rho_1}$ = 2.050), d is the disk diameter, and $\boldsymbol{\rho}$ is the density of the disk;

$$\boldsymbol{d_{33}} = \boldsymbol{K_{31}}\sqrt{\boldsymbol{\epsilon_{33}^T S_{11}^T}} \quad (4)$$

Where $\boldsymbol{\epsilon_{33}^T}$ is the longitudinal permittivity component; $\boldsymbol{S_{11}^T}$ is the elastic compliance.

The hydrothermal-synthesis NBT ceramics (see table.4) were found to have good electrical characteristics ((d_{33}=132 pC/N and kp = 23.17), which were superior to those generated by solid-state techniques. These findings demonstrate that the hydrothermal procedure improves piezoelectric behavior.

Table.5 Piezoelectric properties of specimens produced via the hydrothermal and solid-state methods for NBT

Piezoelectric properties	Hydrothermal method	Solid-state method
$\mathbf{k_p}$	23.17	11.81
$\mathbf{d_{33}}$	132	103

4. Conclusions

In conclusion, (1-x)NBT-xBT solid solution ceramics based on NBT were fabricated using solid-state and hydrothermal techniques with x=0; 0.01; 0.03; 0.05; 0.06; 0.07; 0.08 and 0.1. XRD patterns and Rietveld refinement data for both synthesis techniques indicated the morphotropic phase boundary (MPB) of rhombohedral and tetragonal phases inside the region x=0.05. Raman spectroscopy also revealed the existence of (MPB) in the solid solution. The diverse preparation methods resulted in a microstructure with a significant difference in their average grain size. The NBT sample obtained from the solid structure exhibited an average grain size of ~4 μm, whereas large grains with an average grain size of ~24μm were observed in the NBT sample prepared by the hydrothermal method. The influence of the grain size variation was taken into consideration in the dielectric, ferroelectric, and piezoelectric characteristics. The largest piezoelectric constant d33 of NBT ceramics is about 132 pC/N for those synthesized by the hydrothermal method and the same remark for the dielectric constant. Consequently, both production processes have a specific grain distribution that significantly affects the dielectric and piezoelectric characteristics, due to the internal stresses caused by a large amount of grain boundaries on the grains and the possible hindrance of the domain barrier movements in ceramics developed by the solid-state.

References

[1] M. Shandilya and G. A. Kaur, "Low temperature crystal growth of lead-free complex perovskite nano-structure by using sol-gel hydrothermal process," *J. Solid State Chem.*, vol. 280, p. 120988, Dec. 2019, doi: 10.1016/J.JSSC.2019.120988.

[2] R. Bhattacharyya, S. Das, and S. Omar, "Long-term conductivity stability of acceptor-doped Na0.54Bi0.46TiO3−δ," *Solid State Ionics*, vol. 330, pp. 40–46, Feb. 2019, doi: 10.1016/J.SSI.2018.12.009.

[3] A. Elbasset, F. Abdi, and T. Lamcharfi, "IMPEDANCE SPECTROSCOPY AND PERMITTIVITY STUDY," vol. 66, no. 3, pp. 354–364, 2022, doi: 10.13168/cs.2022.0031.

[4] O. Mezilet, A. Assali, S. Meskine, A. Boukortt, and M. S. Halati, "New insights into the piezoelectric, thermodynamic and thermoelectric properties of lead-free ferroelectric perovskite Na0.5Bi0.5TiO3 from Ab initio calculations," *Mater. Today Commun.*, vol. 31, p. 103371, Jun. 2022, doi: 10.1016/J.MTCOMM.2022.103371.

[5] A. Kumar and S. Asthana, "Beneficial modification of the electrical properties of ecofriendly ferroelectric ceramic Na0.5Bi0.5TiO3 by substitution of low concentration of Ho+3," *Mater. Today Proc.*, vol. 42, pp. 1065–1069, Jan. 2021, doi: 10.1016/J.MATPR.2020.12.168.

[6] W. Wang *et al.*, "Room-temperature multiferroic hexagonal LuFeO3 films," *Phys. Rev. Lett.*, vol. 110, no. 23, Jun. 2013, doi: 10.1103/PHYSREVLETT.110.237601.

[7] T. Takenaka, K. I. Maruyama, and K. Sakata, "(bi1/2na1/2)tio3-bati o3 system for lead-free piezoelectric ceramics," *Jpn. J. Appl. Phys.*, vol. 30, no. 9S, pp. 2236–2239, 1991, doi: 10.1143/JJAP.30.2236.

[8] T. V. Kruzina, V. M. Duda, and J. Suchanicz, "Peculiarities of optical behaviour of Na0.5Bi0.5TiO3 single crystals," *Mater. Sci. Eng. B Solid-State Mater. Adv. Technol.*, vol. 87, no. 1, pp. 48–52, Oct. 2001, doi: 10.1016/S0921-5107(01)00689-4.

[9] M. Mesrar, T. Lamcharfi, N. Echatoui, F. Abdi, and M. Mesrar mohammedmesrar, "Effect of sintering temperature on the microstructure and electrical properties of (Na0.5Bi0.5)TiO3 processed by the sol-gel method," *J. Sol-Gel Sci. Technol. 2022*, pp. 1–12, Jul. 2022, doi: 10.1007/S10971-022-05885-Y.

[10] Y. S. Sung *et al.*, "Effects of Na nonstoichiometry in (Bi 0.5 Na 0.5+x) TiO 3 ceramics," *Appl. Phys. Lett.*, vol. 96, no. 2, 2010, doi: 10.1063/1.3275704.

[11] Z. Wang *et al.*, "Synthesis, structure, dielectric, piezoelectric, and energy storage performance of (Ba0.85Ca0.15)(Ti0.9Zr0.1)O3 ceramics prepared by different methods," *J. Mater. Sci. Mater. Electron.*, vol. 27, no. 5, pp. 5047–5058, May 2016, doi: 10.1007/S10854-

016-4392-X.
[12] M. Afqir *et al.*, "Effect of the synthesis route on the structural and dielectric properties of SrBi1.8Y0.2Nb2O9 ceramics," *Int. J. Miner. Metall. Mater.*, vol. 25, no. 11, pp. 1304–1312, Nov. 2018, doi: 10.1007/S12613-018-1683-7.
[13] R. Kumari, N. Ahlawat, A. Agarwal, S. Sanghi, M. Sindhu, and N. Ahlawat, "Phase transformation and impedance spectroscopic study of Ba substituted Na0.5Bi0.5TiO3 ceramics," *J. Alloys Compd.*, vol. 676, pp. 452–460, Aug. 2016, doi: 10.1016/j.jallcom.2016.03.088.
[14] L. Huang *et al.*, "Effects of Sr doping on the structure, magnetic properties and microwave absorption properties of LaFeO3 nanoparticles," *Ceram. Int.*, vol. 46, no. 17, pp. 27352–27361, Dec. 2020, doi: 10.1016/J.CERAMINT.2020.07.220.
[15] M. J. Pitkethly, "Nanomaterials – the driving force," *Mater. Today*, vol. 7, no. 12, pp. 20–29, Dec. 2004, doi: 10.1016/S1369-7021(04)00627-3.
[16] M. Mesrar, T. Lamcharfi, N.-S. Echatoui, F. Abdi, F. Z. Ahjyaje, and M. Haddad, "Effect of barium doping on electrical and electromechanical properties of (1-x)(Na0.5Bi0.5)TiO3-xBaTiO3," *Mediterr. J. Chem.*, 2019, doi: 10.13171/10.13171/mjc8319050908mm.
[17] M. M. Sidi, M. Ben, and F. A. Sidi, "Investigation of Morphotropic Phase Boundary by Rietveld Refinement and Raman Spectroscopy for (1-x)(Na0.5Bi0.5)TiO3-xBaTiO3 Ceramics ASIAN JOURNAL OF CHEMISTRY ASIAN JOURNAL OF CHEMISTRY," 2018, doi: 10.14233/ajchem.2018.21116.
[18] M. Spreitzer, M. Valant, D. S.-J. of M. Chemistry, and undefined 2007, "Sodium deficiency in Na 0.5 Bi 0.5 TiO 3," *pubs.rsc.org*.
[19] W. Huang *et al.*, "Structural, ferroelectric, and optical properties of Pr-NBT-xCTO relaxor ferroelectric thin films," *Ceram. Int.*, vol. 45, no. 8, pp. 10475–10480, Jun. 2019, doi: 10.1016/j.ceramint.2019.02.109.
[20] E. Aksel and J. L. Jones, "Phase formation of sodium bismuth titanate perovskite during solid-state processing," *J. Am. Ceram. Soc.*, vol. 93, no. 10, pp. 3012–3016, Oct. 2010, doi: 10.1111/j.1551-2916.2010.03977.x.
[21] X. Yang *et al.*, "Formation mechanism of CaTiO3 hollow crystals with different microstructures," *J. Am. Chem. Soc.*, vol. 132, no. 40, pp. 14279–14287, Oct. 2010, doi: 10.1021/JA106461U.
[22] I. Coondoo *et al.*, "A comparative study of structural and electrical properties in lead-free BCZT ceramics: Influence of the synthesis method," *Acta Mater.*, vol. 155, pp. 331–342, Aug. 2018, doi: 10.1016/J.ACTAMAT.2018.05.029.
[23] Z. Sun *et al.*, "Impact of fast microwave sintering on the grain growth, dielectric relaxation and piezoelectric properties on Ba0.18Ca0.02Ti0.09Zr0.10O3 lead-free ceramics prepared by different methods," *Mater. Sci. Eng. B*, vol. 185, no. 1, pp. 114–122, Jul. 2014, doi: 10.1016/J.MSEB.2014.02.016.
[24] H. Lidjici, B. Marfoua, B. Laghoun, M. Rguitti, and H. Khemakhem, "Dielectric properties and relaxor behavior of 0.935(Na0.5Bi0.5)TiO3-0.065BaTiO3 lead free piezoelectric ceramic," *Ceram. Int.*, vol. 42, no. 11, pp. 12735–12739, Aug. 2016, doi: 10.1016/J.CERAMINT.2016.05.029.
[25] M. Mesrar, T. Lamcharfi, N. S. Echatoui, and F. Abdi, "(1-x)(Na0.5Bi0.5)TiO3-x(K0.5Bi0.5)TiO3 ceramics near morphotropic phase boundary: A structural and electrical study," *Materialia*, vol. 22, p. 101404, May 2022, doi: 10.1016/J.MTLA.2022.101404.
[26] M. Mesrar, T. Lamcharfi, N. Echatoui, F. Abdi, A. Harrach, and F. Z. Ahjyaje, "Hydrothermal synthesis, microstructure and electrical properties of (1- x)(Na0.5Bi0.5)TiO3-xBaTiO3 ceramics," *Moroccan J. Quant. Qual. Res.*, vol. 0, no. 1, pp. 14–24, 2019.
[27] K. Qian *et al.*, "Construction of Bi2Ti2O7/Bi4Ti3O12 composites with enhanced visible light photocatalytic activity," *Mater. Lett.*, vol. 206, pp. 245–248, Nov. 2017, doi: 10.1016/J.MATLET.2017.07.036.
[28] A. Amouri, H. Abdelkefi, N. Abdelmoula, and H. Khemakhem, "Phase transition behavior and ferroelectric and vibrational properties of (Na0.5Bi0.5)1−xBaxTi1−x(Fe0.5Nb0.5)xO3 ceramics," *J. Mater. Sci.*, vol. 52, no. 7, pp. 3876–3892, Apr. 2017, doi: 10.1007/S10853-016-

0649-2/FIGURES/9.

[29] Y. D. Hou, L. Hou, S. Y. Huang, M. K. Zhu, H. Wang, and H. Yan, "Comparative study of K0.5Bi0.5TiO3 nanoparticles derived from sol–gel-hydrothermal and sol–gel routes," *Solid State Commun.*, vol. 137, no. 12, pp. 658–661, Mar. 2006, doi: 10.1016/J.SSC.2006.01.023.

[30] G. Bergerhoff, M. Berndt, and K. Brandenburg, "Evaluation of Crystallographic Data with the Program DIAMOND," *J. Res. Natl. Inst. Stand. Technol.*, vol. 101, no. 3, p. 221, May 1996, doi: 10.6028/JRES.101.023.

[31] W. Kang, Z. Zheng, Y. Li, and R. Zhao, "Enhanced dielectric and piezoelectric performance of sol-gel derived (1-x) Bi0.5(Na0.78K0.22)0.5TiO3-xBaTiO3 ceramics," *Ceram. Int.*, vol. 45, no. 17, pp. 23078–23083, Dec. 2019, doi: 10.1016/J.CERAMINT.2019.07.356.

[32] J. F. Peng, X. J. Zheng, Y. Q. Gong, K. Zhan, and Z. H. Dai, "Effects of Annealing Temperature on the Electric Properties of 0.94(Na 0.5 Bi 0.5)TiO 3-0.06BaTiO 3 Ferroelectric Thin Film," doi: 10.1007/s11664-013-2912-5.

[33] Q. Liu *et al.*, "Effect of the Yb3+ Concentration in Up-Conversion and Electrical Properties of Ho3+/Yb3+ Co-doped (0.94Na0.5Bi0.5TiO3-0.06BaTiO3) Ceramics," *J. Electron. Mater. 2016 457*, vol. 45, no. 7, pp. 3473–3478, Apr. 2016, doi: 10.1007/S11664-016-4483-8.

[34] M. Mesrar, T. Lamcharfi, N.-S. Echatoui, and F. Abdi, "(1-x)(Na0.5Bi0.5)TiO3-x(K0.5Bi0.5)TiO3 ceramics near morphotropic phase boundary: a structural and electrical study," *Materialia*, p. 101404, Mar. 2022, doi: 10.1016/J.MTLA.2022.101404.

[35] M. Mesrar, T. Lamcharfi, N. S. Echatoui, F. Abdi, and F. Z. Ahjyaje, "Hydrothermal synthesis of oxide and carbonate powders of (1-x)(na0.5bi0.5)tio3-xbatio3 ceramics," *Asian J. Chem.*, vol. 31, no. 2, pp. 309–316, 2019, doi: 10.14233/AJCHEM.2019.21581.

[36] M. Mesrar, T. Lamcharfi, N.-S. Echatoui, F. Abdi, and A. Harrach, "High dielectric constant of (1-x)(Na0.5Bi0.5)TiO3-xBaTiO3 prepared by the hydrothermal method," *Mediterr. J. Chem.*, 2019, doi: 10.13171/10.13171/mjc8319051210mm.

[37] G. Liu *et al.*, "An Investigation of Dielectric, Piezoelectric Properties and Microstructures of Bi0.5Na0.5TiO3-BaTiO3-Bi0.5K0.5TiO3 Lead-Free Piezoelectric Ceramics Doped with K2AlNbO5 Compound," *J. Electron. Mater. 2017 468*, vol. 46, no. 8, pp. 5287–5295, May 2017, doi: 10.1007/S11664-017-5545-2.

[38] J. Petzelt *et al.*, "Infrared, Raman and high-frequency dielectric spectroscopy and the phase transitions in Na1/2Bi1/2TiO3," *J. Phys. Condens. Matter*, vol. 16, no. 15, pp. 2719–2731, Apr. 2004, doi: 10.1088/0953-8984/16/15/022.

[39] Y. Wang *et al.*, "Hydrothermal synthesis and characterization of Na0.5Bi0.5TiO3 microcubes," *Ceram. Int.*, vol. 35, no. 4, pp. 1657–1659, May 2009, doi: 10.1016/j.ceramint.2008.07.018.

[40] W. Cai, C. Fu, W. Hu, G. Chen, and X. Deng, "Effects of microwave sintering power on microstructure, dielectric, ferroelectric and magnetic properties of bismuth ferrite ceramics," *J. Alloys Compd.*, vol. 554, pp. 64–71, Mar. 2013, doi: 10.1016/J.JALLCOM.2012.11.154.

[41] P. Parjansri, M. Kamnoy, and S. Eitssayeam, "Electrical Properties of Lead-Free (Bi0.5Na0.5)TiO3 Piezoelectric Ceramics Induced by BNT Nanoparticles," *J. Electron. Mater. 2021 513*, vol. 51, no. 3, pp. 1068–1076, Jan. 2022, doi: 10.1007/S11664-021-09351-3.

[42] Z. Wu *et al.*, "Effects of Mg Doping on Microstructure and Dielectric and Ferroelectric Properties of Lead-Free NaBiTi6O14 Ceramics," *J. Electron. Mater. 2019 488*, vol. 48, no. 8, pp. 5226–5232, Jun. 2019, doi: 10.1007/S11664-019-07293-5.

[43] C. H. Yang *et al.*, "Properties of Na0.55Bi0.55TiO3 ferroelectric films prepared by chemical solution decomposition," *Growth*, vol. 284, no. 1–2, pp. 136–141, Oct. 2005, doi: 10.1016/j.jcrysgro.2005.06.038.

[44] B. J. Chu, D. R. Chen, G. R. Li, and Q. R. Yin, "Electrical properties of Na1/2Bi1/2TiO3-BaTiO3 ceramics," *J. Eur. Ceram. Soc.*, vol. 22, no. 13, pp. 2115–2121, 2002, doi: 10.1016/S0955-2219(02)00027-4.

[45] C. Huang *et al.*, "Effect of preparation process on properties of PLZT (9/65/35) transparent ceramics," *J. Alloys Compd.*, vol. 723, pp. 602–610, Nov. 2017, doi: 10.1016/J.JALLCOM.2017.06.271.

[46] X. Liu, J. Zhai, B. Shen, F. Li, and P. Li, "Structural Transition and Electrical Properties of (1 − x)(Na0.4K0.1Bi0.5)TiO3-xSrTiO3 Lead-Free Piezoceramics," *J. Electron. Mater. 2017 4610*, vol. 46, no. 10, pp. 5553–5562, Jun. 2017, doi: 10.1007/S11664-017-5648-9.